We are IntechOpen, the world's leading publisher of Open Access books
Built by scientists, for scientists

4,800
Open access books available

122,000
International authors and editors

135M
Downloads

Our authors are among the

154
Countries delivered to

TOP 1%
most cited scientists

12.2%
Contributors from top 500 universities

CLARIVATE ANALYTICS
BOOK CITATION INDEX
INDEXED

WEB OF SCIENCE™

Selection of our books indexed in the Book Citation Index in Web of Science™ Core Collection (BKCI)

Interested in publishing with us?
Contact book.department@intechopen.com

Numbers displayed above are based on latest data collected.
For more information visit www.intechopen.com

Chapter 4

Operational Modal Analysis of Super Tall Buildings by a Bayesian Approach

Feng-Liang Zhang and Yan-Chun Ni

Additional information is available at the end of the chapter

http://dx.doi.org/10.5772/intechopen.68397

Abstract

Structural health monitoring (SHM) has attracted increasing attention in the past few decades. It aims at monitoring the existing structures based on data acquired by different sensor networks. Modal identification is usually the first step in SHM, and it aims at identifying the modal parameters mainly including natural frequency, damping ratio and mode shape. Three different field tests can be used to collect data for modal identification, among which, ambient vibration test is the most convenient and economical one since it does not require to measure input information. This chapter will focus on the operational modal analysis (OMA), i.e. ambient modal identification of four super tall buildings by a Bayesian approach. A fast frequency domain Bayesian fast fourier transform (FFT) approach will be introduced for OMA. In addition to the most probable value (MPV) of modal parameters, the associated posterior uncertainty will be also investigated analytically. The field tests will be presented and the difficulties encountered will be discussed. Some basic dynamic characteristics will be investigated and discussed. The studies will provide baseline properties of these super tall buildings and provide a reference for future condition assessments.

Keywords: structural health monitoring, operational modal analysis, ambient vibration test, super tall buildings, posterior uncertainty, Bayesian method

1. Introduction

Structural health monitoring has attracted increasing attention in the past few decades [1–3]. In the past decade, much more super tall buildings have been constructed and most of them were instrumented structural health monitoring (SHM) systems, for example, Canton Tower with the height of 610 m, on which more than 700 sensors were installed to form a sophisticated long-term SHM systems [3, 4]; Burj Khalifa, the tallest building in the world with the height of

INTECH
open science | open minds

© 2017 The Author(s). Licensee InTech. This chapter is distributed under the terms of the Creative Commons Attribution License (http://creativecommons.org/licenses/by/3.0), which permits unrestricted use, distribution, and reproduction in any medium, provided the original work is properly cited. CC BY

828 m, on which an integrated real-time SHM system was instrumented [5]; Shanghai Tower with the height of 632 m and so on. Some super tall buildings are still under construction, such as Pingan International Financial Center with a height of 660 m, Shenzhen, China; Wuhan Greenland Center with a height of 636 m, Wuhan, China; Kingdom Tower with the height of 1007 m, Jeddah, Saudi Arabia. These systems play an important role in monitoring the structural conditions and making an assessment when extreme events happen. For some super tall buildings, although their heights are also more than 300 m, no long-term SHM systems were installed. Some short-term monitoring was also carried out [6, 7], for example, Building A with the height of 310 m, Hong Kong; Building B with the height of 320 m, Hong Kong; International Finance Centre with the height of 416 m, Hong Kong; etc. When some typhoons came, vibration data were collected to investigate the dynamic characteristics of these buildings.

For these super tall buildings, the monitoring of acceleration response plays an important role since the dynamic characteristics mainly including natural frequencies, damping ratios and modes shapes can be determined. They are the typical characteristics of the structures and will remain unchanged if there is no significant damage and can be used for model updating, damage detection and SHM [8–10]. The natural frequencies can help to find potential vibration problem, e.g. resonance, and then some measures can be designed to alleviate them. The damping ratio can affect the vibration level and energy dissipation capability of the structure. In the structure designing, this quantity is usually set to be constant, e.g., 5%. However, in reality, it can be affected by many factors, for example, vibration amplitude. Therefore, knowing damping ratio can better assess the structural response and provides a reference in the structural design. The mode shapes can reflect the stiffness and mass distribution and the boundary conditions of objective structures, whose change across extreme events can be used for damage detection and SHM.

To obtain the modal parameters, modal identification needs to be carried out using structural response. Acceleration and velocity data are commonly used for modal identification. There are three main ways to collect structural responses, which are free vibration test, forced vibration test and ambient vibration test. The first one is to collect structural response when the structure is under free vibration dominantly. However, for the structures in civil engineering, it is usually difficult for them to vibrate freely. The second one is to collect structural response when given some known excitation during the test. This method can improve the vibration level and provide a high signal to noise ratio for the structural response. However, to produce forced vibration, special equipment such as a high payload shaker is required. This makes the test expensive and some unexpected damage may be caused if the equipment cannot be well controlled. The third one, compared with the former two tests, is more convenient and economical since no additional excitations are required. The excitations are mainly from the ambient loading, e.g. wind, traffic loading, human walking, environmental noise, and so on. For this test, it requires high quality sensors with a lower noise level to improve the signal to noise ratio. If the noise level is too high, the modal parameters identified may have higher uncertainty.

Ambient modal identification, also called operational modal analysis (OMA), can be used to obtain the modal parameters using ambient vibration data [11]. The excitation is usually assumed to be stochastic stationary. Many methods have been developed for OMA, for example, stochastic subspace identification (SSI) [12], peak-picking (PP), and frequency domain decomposition (FDD) [13]. In addition to these non-Bayesian methods, a series of Bayesian

methods have been developed [14–15], for example, Bayesian spectral density approach, Bayesian time domain method, and Bayesian fast fourier transform (FFT) approach. Recently, a fast Bayesian FFT method has been developed based on Bayesian FFT approach [16–20]. It has been extended to forced vibration data [21], free vibration data [22–23], and so on. This method views modal identification as an inference problem where the probability is taken as a measure for the relative plausibility of outcomes given a model of the structure and measured data. Both the most probable value (MPV) and the associated posterior uncertainty can be determined, making it possible to assess the accuracy of the identified modal parameters.

Based on the technique of OMA, many super tall buildings have been studied, for example, Canton Tower, super tall buildings in Hong Kong, and so on. This chapter presents the work on OMA of four different super tall buildings, including two super tall buildings in Hong Kong, Canton Tower and Shanghai Tower. It is organized as follows. In Section 2, the fast Bayesian FFT method will be introduced and it will be used for the latter study in the MPV and the associated posterior uncertainty. In Section 3, the OMA of two super tall buildings in Hong Kong will be presented. The data were collected during different strong wind events. The amplitude-dependence behaviour of modal parameters was investigated. In Section 4, Canton Tower was studied using the data collected during one day's measurement by the SHM system installed. In Section 5, Shanghai Tower, the second tallest building in the world until now, was investigated by ambient vibration tests in different stages. Finally, the summary is given in Section 6.

2. Fast Bayesian FFT method

2.1. Bayesian method for single setup

A fast Bayesian FFT approach is employed to identify the modal properties of the instrumented building using the recorded ambient vibration data in a single setup. The theory is briefly described here. The reader is referred to Ref. [14] for the original formulation and to Refs. [11, 16–18] for a recently developed fast algorithm that allows practical implementation.

The measured acceleration data are assumed to consist of the structural ambient vibration signal and prediction error

$$\ddot{\mathbf{y}}_j = \ddot{\mathbf{x}}_j + \mathbf{e}_j \tag{1}$$

where $\ddot{\mathbf{x}}_j \in R^n$ and $\mathbf{e}_j \in R^n$ (j = 1,2,…, N), respectively, denote the theoretical structural acceleration response and the prediction error, n measured degrees of freedom (DOFs), N the sampling points number. The FFT of the collected data $\ddot{\mathbf{y}}_j$ is given by

$$\mathcal{F}_k = \sqrt{\frac{2\Delta t}{N}} \sum_{j=1}^{N} \ddot{\mathbf{y}}_j \exp\left[-2\pi \mathbf{i} \frac{(k-1)(j-1)}{N}\right] \tag{2}$$

in which $\mathbf{i}^2 = -1$, Δt the sampling interval, $k = 1, \ldots, N_q$ with $N_q = \text{int}[N/2] + 1$, int[.] the integer part.

Let $\boldsymbol{\theta}$ denote the targeted modal parameters, including f_i, ζ_i, $\boldsymbol{\varphi}_i$, $i = 1, \ldots, m$ (m is the number of modes), where f_i and ζ_i denote, respectively, the natural frequency and damping ratio of the i-th mode, and $\boldsymbol{\varphi}_i \in R^n$ is the i-th mode shape vector; $\mathbf{S} \in R^{m \times m}$, S_e, the (symmetric) power spectral density (PSD) of modal forces and the PSD of prediction error, respectively.

Let $\mathbf{Z}_k = [\mathrm{Re}\mathcal{F}_k; \mathrm{Im}\mathcal{F}_k] \in R^{2n}$ denote the real and imaginary parts of the FFT data at f_k, where f_k is the FFT frequency abscissa. When performing the modal identification, the FFT data in a selected frequency band are used and they are denoted by $\{\mathbf{Z}_k\}$. Based on Bayes' theorem, the posterior probability density function (PDF) of $\boldsymbol{\theta}$ can be expressed as

$$p(\boldsymbol{\theta}|\{\mathbf{Z}_k\}) \propto p(\boldsymbol{\theta}) p(\{\mathbf{Z}_k\}|\boldsymbol{\theta}) \tag{3}$$

in which $p(\boldsymbol{\theta})$ denotes the prior PDF. The prior information is assumed to be uniform, and so the posterior PDF can be taken to be proportional to the 'likelihood function' $p(\{\mathbf{Z}_k\}|\boldsymbol{\theta})$ directly. The 'most probable value' (MPV) of $\boldsymbol{\theta}$ can be obtained by maximizing $p(\{\mathbf{Z}_k\}|\boldsymbol{\theta})$.

When N is large and Δt is small, the FFT can be shown to be asymptotically independent at different frequencies and follows a Gaussian distribution [14]. Therefore, $p(\{\mathbf{Z}_k\}|\boldsymbol{\theta})$ can be expressed as

$$p(\{\mathbf{Z}_k\}|\boldsymbol{\theta}) = \prod_k \frac{1}{(2\pi)^n (\det \mathbf{C}_k)^{1/2}} \exp\left[-\frac{1}{2} \mathbf{Z}_k{}^T \mathbf{C}_k{}^{-1} \mathbf{Z}_k\right] \tag{4}$$

in which det(.) denotes the determinant, $\mathbf{C}_k$ the covariance matrix of $\mathbf{Z}_k$ given by

$$\mathbf{C}_k = \frac{1}{2} \begin{bmatrix} \boldsymbol{\Phi} & \\ & \boldsymbol{\Phi} \end{bmatrix} \begin{bmatrix} \mathrm{Re}\mathbf{H}_k & -\mathrm{Im}\mathbf{H}_k \\ \mathrm{Im}\mathbf{H}_k & \mathrm{Re}\mathbf{H}_k \end{bmatrix} \begin{bmatrix} \boldsymbol{\Phi}^T & \\ & \boldsymbol{\Phi}^T \end{bmatrix} + \frac{S_e}{2} \mathbf{I}_{2n} \tag{5}$$

and $\mathbf{I}_{2n} \in R^{2n}$ denotes the identity matrix, $\boldsymbol{\Phi} = [\boldsymbol{\varphi}_1, \boldsymbol{\varphi}_2, \ldots, \boldsymbol{\varphi}_m] \in R^{n \times m}$ the mode shape matrix, $\mathbf{H}_k \in R^{m \times m}$ the transfer matrix, and its (i, j) element can be given by

$$\mathbf{H}_k(i,j) = S_{ij} \left[\left(\beta_{ik}^2 - 1\right) + 2\mathbf{i}\zeta_i \beta_{ik}\right]^{-1} \left[\left(\beta_{jk}^2 - 1\right) - 2\mathbf{i}\zeta_j \beta_{jk}\right]^{-1} \tag{6}$$

and $\beta_{ik} = f_i / f_k$; f_i is the natural frequency of the i-th mode; S_{ij} is the cross spectral density between the i-th and j-th modal excitation. The first and second term in Eq. (5) represent the contribution from the modal response and the prediction error, respectively.

Theoretically, the modal parameters can be determined by maximizing the posterior PDF. However, there are some computational difficulties. To develop an efficient algorithm, a fast algorithm was developed, and it allows the MPV and the associated posterior uncertainty to be obtained efficiently [16–18].

2.2. Bayesian method for multiple setups

In full-scale ambient tests, usually there are a large number of DOFs to be measured, but the number of available sensors is often limited. In this part, a fast Bayesian method for modal

identification of well separated modes incorporating data from multiple setups will be presented. For the details of this part, please refer to [11, 19, 20].

Assume that in a selected frequency band, there is only one contributing mode and $\boldsymbol{\varphi} \in R^n$ denotes the global mode shape containing all the DOFs of interest. To relate the $\boldsymbol{\varphi}$ to the mode shape in a given setup covering a possibly different set of DOFs, the selection matrix in Setup i $(i = 1, \ldots, n_s)$, $\mathbf{L}_i \in R^{n_i \times n}$ will be defined and n_i denotes the number of measured DOFs in Setup i. In Setup i, the (j,k) entry of $\mathbf{L}_i$ is set to 1 when DOF k is measured by the j-th channel, and it is equal to zero for the other situations. The theoretical mode shape confined to the measured DOFs in Setup i can be given by $\boldsymbol{\varphi}_i = \mathbf{L}_i \boldsymbol{\varphi} \in R^{n_i}$. The modal parameters to be identified are defined as

$$\boldsymbol{\theta} = [f_i, \zeta_i, S_i, S_{ei} : i = 1, \ldots, n_s; \boldsymbol{\varphi} \in R^n] \in R^{4n_s+n} \tag{7}$$

in which $f_i, \zeta_i, S_i, S_{ei} (i = 1, \ldots, n_s)$ denote the modal parameters in Setup i.

Let $\mathbf{Z}_k^{(i)} = [\mathrm{Re}\mathcal{F}_{ik}; \mathrm{Im}\mathcal{F}_{ik}] \in R^{2n_i} (i = 1, \ldots, n_s)$ denote the FFT data at frequency f_k in the i-th setup; $\mathcal{D}_i = \{\mathbf{Z}_k^{(i)}\}$ denote the FFT data in a selected frequency band in Setup i and $\mathcal{D} = \{\mathcal{D}_i : i = 1, \ldots, n_s\}$ denote the FFT data in all the setups. Assuming the data in different setups are independent, based on Bayes' Theorem, given the data in all setups, the posterior PDF of $\boldsymbol{\theta}$ is given by

$$p(\boldsymbol{\theta}|\mathrm{D}) \propto p(\{D_1, D_2, \ldots, D_{n_s}\}|\boldsymbol{\theta}) = p(D_1|\boldsymbol{\theta}) p(D_2|\boldsymbol{\theta}) \ldots p(D_{n_s}|\boldsymbol{\theta}) \tag{8}$$

Note that $p(\mathcal{D}_i|\boldsymbol{\theta})$ is independent with the modal parameters in other setups, and so $p(\mathcal{D}_i|\boldsymbol{\theta}) = p(\mathcal{D}_i|f_i, \zeta_i, S_i, S_{ei}, \boldsymbol{\varphi}_i)$. Eq. (8) can be given by

$$p(\boldsymbol{\theta}|\mathcal{D}) \propto \prod_{i=1}^{n_s} p(\mathcal{D}_i|f_i, \zeta_i, S_i, S_{ei}, \boldsymbol{\varphi}_i) \tag{9}$$

Similar to above section, $p(\mathcal{D}_i|f_i, \zeta_i, S_i, S_{ei}, \boldsymbol{\varphi}_i)$ is asymptotically a Gaussian distribution, with negative log-likelihood function (NLLF)

$$L_i(\boldsymbol{\theta}_i) = \frac{1}{2} \sum_k \left[\ln \det \mathbf{C}_{ik}(\boldsymbol{\theta}_i) + \mathbf{Z}_k^{(i)T} \mathbf{C}_{ik}(\boldsymbol{\theta}_i)^{-1} \mathbf{Z}_k^{(i)} \right] \tag{10}$$

in which $\boldsymbol{\theta}_i = \{f_i, \zeta_i, S_i, S_{ei}, \boldsymbol{\varphi}_i\}$ and

$$\mathbf{C}_{ik}(\boldsymbol{\theta}_i) = \frac{S_i D_{ik}}{2} \begin{bmatrix} \boldsymbol{\varphi}_i \boldsymbol{\varphi}_i^T & 0 \\ 0 & \boldsymbol{\varphi}_i \boldsymbol{\varphi}_i^T \end{bmatrix} + \frac{S_{ei}}{2} \mathbf{I}_{2n_i} \tag{11}$$

is the theoretical covariance matrix of the FFT data at the k-th frequency abscissa in Setup i, in which

$$D_{ik}(f_i, \zeta_i) = \left[(\beta_{ik}^2 - 1)^2 + (2\zeta_i\beta_{ik})^2\right]^{-1} \tag{12}$$

with $\beta_{ik} = f_i/\mathrm{f}_k$. Consequently,

$$p(\boldsymbol{\theta}|\mathcal{D}) \propto \exp\left(-L(\boldsymbol{\theta})\right) \tag{13}$$

in which

$$L(\boldsymbol{\theta}) = \sum_{i=1}^{n_s} L_i(\boldsymbol{\theta}_i) \tag{14}$$

Similar to the case in single setup in Section 2.1., there are some computational difficulties. For the purpose of developing a fast computational procedure, it is found det$\mathbf{C}_{ik}$ and $\mathbf{C}_{ik}^{-1}$ can be analysed and obtained in a more manageable form. As a result (proof omitted here), the overall NLLF can be reformulated as

$$\begin{aligned} L(\boldsymbol{\theta}) &= -(\ln 2)\sum_{i=1}^{n_s} n_i N_{fi} + \sum_{i=1}^{n_s}(n_i - 1)N_{fi}\ln S_{ei} \\ &+ \sum_{i=1}^{n_s}\sum_{k}\ln(S_i D_{ik}\|\mathbf{L}_i\boldsymbol{\varphi}\|^2 + S_{ei}) + \sum_{i=1}^{n_s} S_{ei}^{-1} d_i - \boldsymbol{\varphi}^T\mathbf{A}(\boldsymbol{\varphi})\boldsymbol{\varphi} \end{aligned} \tag{15}$$

where

$$\mathbf{A}(\boldsymbol{\varphi}) = \sum_{i=1}^{n_s} S_{ei}^{-1}\sum_{k}(\|\mathbf{L}_i\boldsymbol{\varphi}\|^2 + \frac{S_{ei}}{S_i D_{ik}})^{-1}\mathbf{L}_i^T\mathbf{D}_{ik}\mathbf{L}_i \in R^{n\times n} \tag{16}$$

$$\mathbf{D}_{ik} = \mathrm{Re}\mathcal{F}_{ik}\mathrm{Re}\mathcal{F}_{ik}{}^T + \mathrm{Im}\mathcal{F}_{ik}\mathrm{Im}\mathcal{F}_{ik}{}^T \in R^{n_i\times n_i} \tag{17}$$

$$d_i = \sum_{k}(\mathrm{Re}\mathcal{F}_{ik}{}^T\mathrm{Re}\mathcal{F}_{ik} + \mathrm{Im}\mathcal{F}_{ik}{}^T\mathrm{Im}\mathcal{F}_{ik}) \tag{18}$$

Based on Eq. (15), an iterative scheme for the full set of solution of modal parameters can be developed, which makes the identification of modal parameters very efficiently even for a large number of measured DOFs. The associated posterior uncertainties can be calculated by the analytical formulas without resorting to finite difference. Details can be found in Refs. [19, 20].

3. Two super tall buildings in Hong Kong

Buildings A and B are two super tall buildings in Hong Kong. Building A is 310 m tall, 50 m by 50 m in plan, which is a tabular concrete building with a central core wall system. Building B is 320 m tall, 50 m × 50 m in plan, whose lateral structural resistance is provided by two outrigger trusses with core walls near the centre and mega columns at the corner. **Figure 1** shows the mode

http://dx.doi.org/10.5772/intechopen.68397

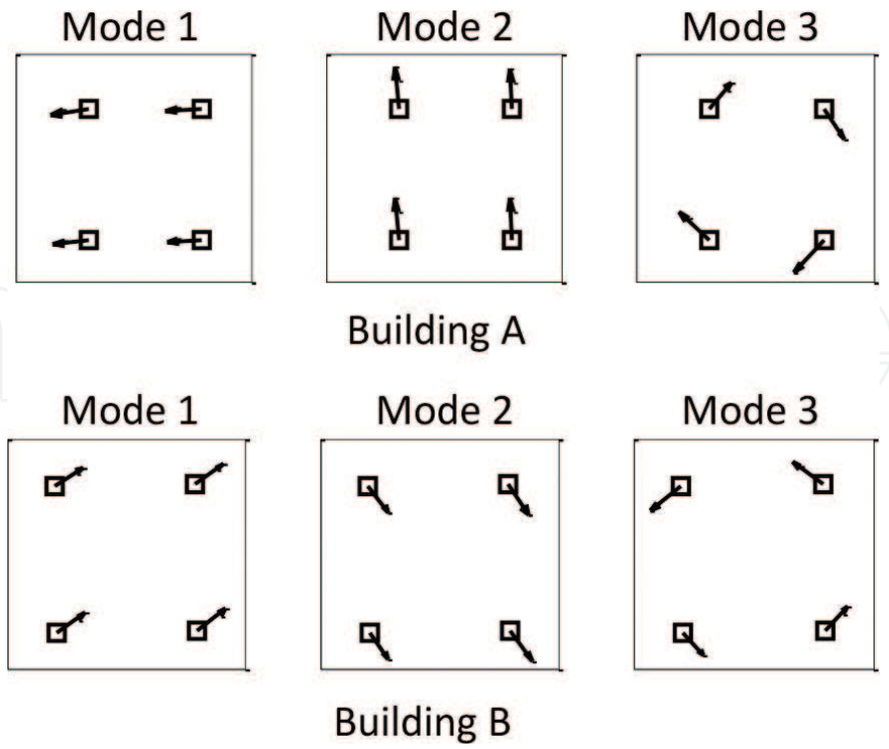

Figure 1. Mode shapes of Buildings A and B identified under normal wind.

shapes of the first three modes of Buildings A and B. They were identified based on ambient data by placing four tri-axial accelerometers at four corners on the roof. The two numbers near to the mode name are the natural frequency and damping ratio, respectively. For Building B, due to connection to a neighbouring building, the principal modal directions do not align with the building sides.

Figure 2 shows the sensor layout inside the rooms on the roof of the buildings, and the sensor locations were kept the same for all the typhoon events. The vibration data investigated were measured during two typhoon events (namely, Typhoon Goni and Koppu) and two monsoon events (MS1 and MS2). Typhoon Goni attacked Hong Kong during 4–6 August 2009. The wind speed changed between 22 and 60 km/hr. One month later, Typhoon Koppu attacked Hong Kong. Koppu travelled faster than Goni. The wind speed changed between 25 and 120 km/hr. Typhoon Koppu provides much more information due to large structural vibrations in the current study. The MS1 visited during 4–7 January 2010. The wind speed changed between 15 and 50 km/hr. The MS2 visited in December 2010. The wind speed ranged between 12 and 45 km/hr. The wind speeds in the two monsoon events are significantly lower than those in the typhoon events. The typhoon events can provide information for large amplitude vibration study, while the monsoon events can provide information in the low to moderate wind speed regime.

The recorded acceleration data are used for identifying the modal parameters of the structures by the Bayesian method. For the purpose that the loading and the response can be modelled as stationary stochastic process, the whole time history is divided into non-overlapping time windows of 30 minutes. **Figure 3** shows the singular value (SV) spectra of the first half hour data of Building A during Typhoon Koppu. Six modes below 1 Hz can be observed while the

(a) Building A (b) Building B

Figure 2. Equipment used during strong wind event.

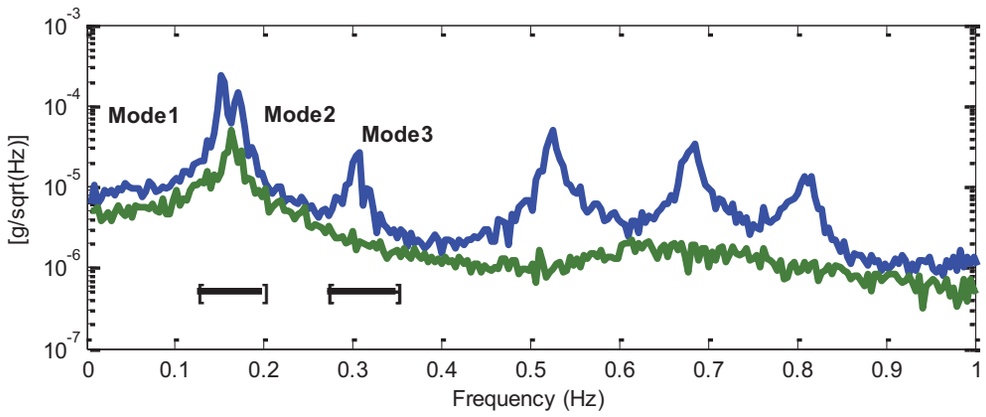

Figure 3. Root singular value spectra, 30-minute acceleration data, Building A.

first two modes are closely spaced. Similarly, in Building B, whose SV spectra is omitted here, there are also six modes below 1 Hz and the first two modes are closely spaced modes. The closely spaced modes may be due to their square-shaped floor plan of Buildings A and B. The first three modes are investigated including the first two translational modes and the first torsional mode.

Table 1 shows the modal parameters for Building A. The MPV of modal parameters and the corresponding posterior coefficient of variations (c.o.v.) are provided in the table. The posterior c.o.v.s of the natural frequencies are all less than 1%, which are much smaller than those of the damping ratio or the PSD of modal force. The posterior uncertainty of the damping ratio governs the data length requirement and with 30 minutes of data its c. o.v. is about 30%, showing a moderate level of accuracy. Similar investigation to Building B is also performed.

Next, the correlation between the identified natural frequencies and damping ratios with the vibration amplitude calculated based on Ref. [6] is investigated. **Figures 4** and **5**, respectively, show the MPV of natural frequencies and damping ratios versus the modal vibration root-mean-square (RMS) for Buildings A and B. The results for all time windows in four different events are plotted in the figure. A circle, a cross and a triangle denote the results for Typhoon Goni, Typhoon Koppu and MS2, respectively, in Building A, while for Building B, a cross and a

Mode	f (Hz)		ζ (%)		S [$(\mu g)^2$/Hz]	
	MPV	**(c.o.v.)**	**MPV**	**(c.o.v.)**	**MPV**	**(c.o.v.)**
TX1	0.153	(0.16%)	0.5	(36%)	225.4	(9.0%)
TX2	0.170	(0.31%)	1.7	(20%)	349.1	(10%)
R1	0.302	(0.17%)	0.9	(20%)	4.5	(10%)

Table 1. Summary of identified modal properties, building A, first 30 minutes in Koppu.

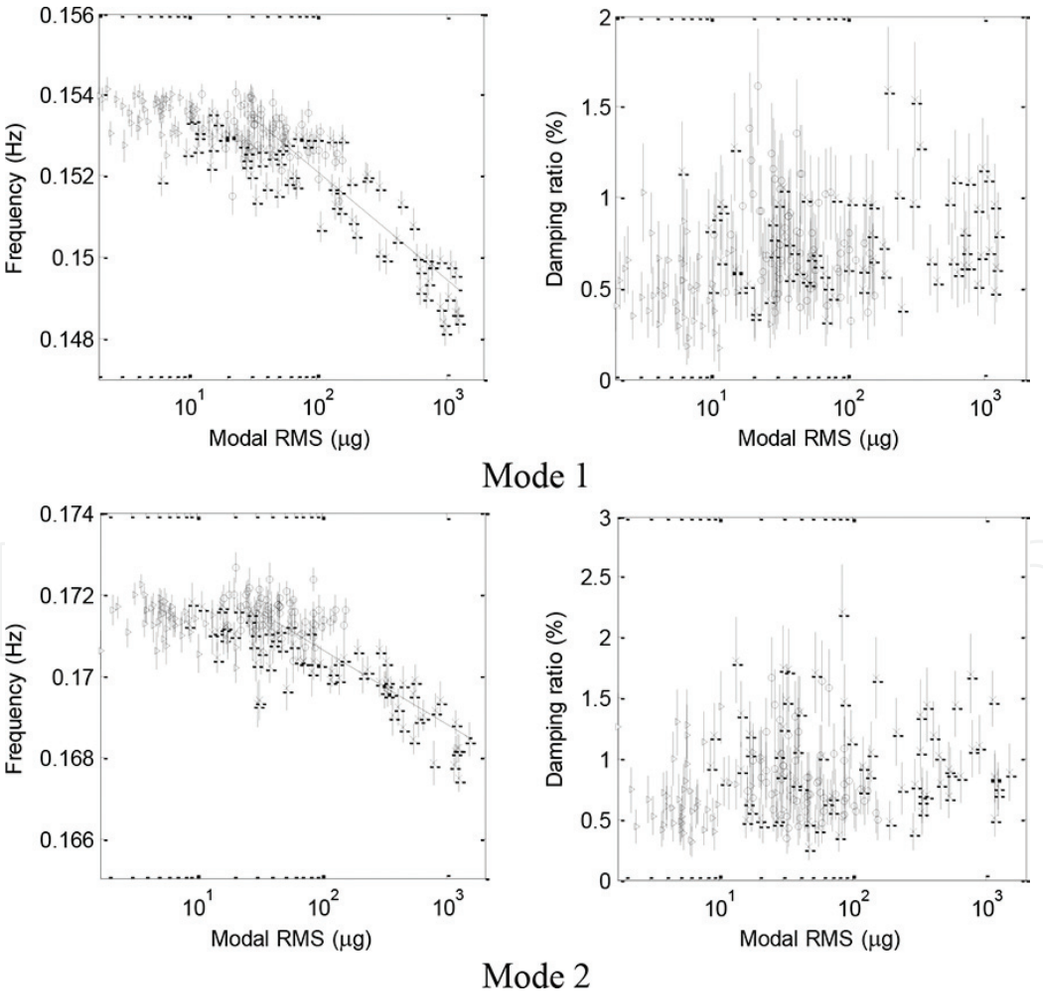

Figure 4. Identified modal frequency and damping ratio versus modal RMS of Building A (o: Goni; ×: Koppu; ▷: MS2).

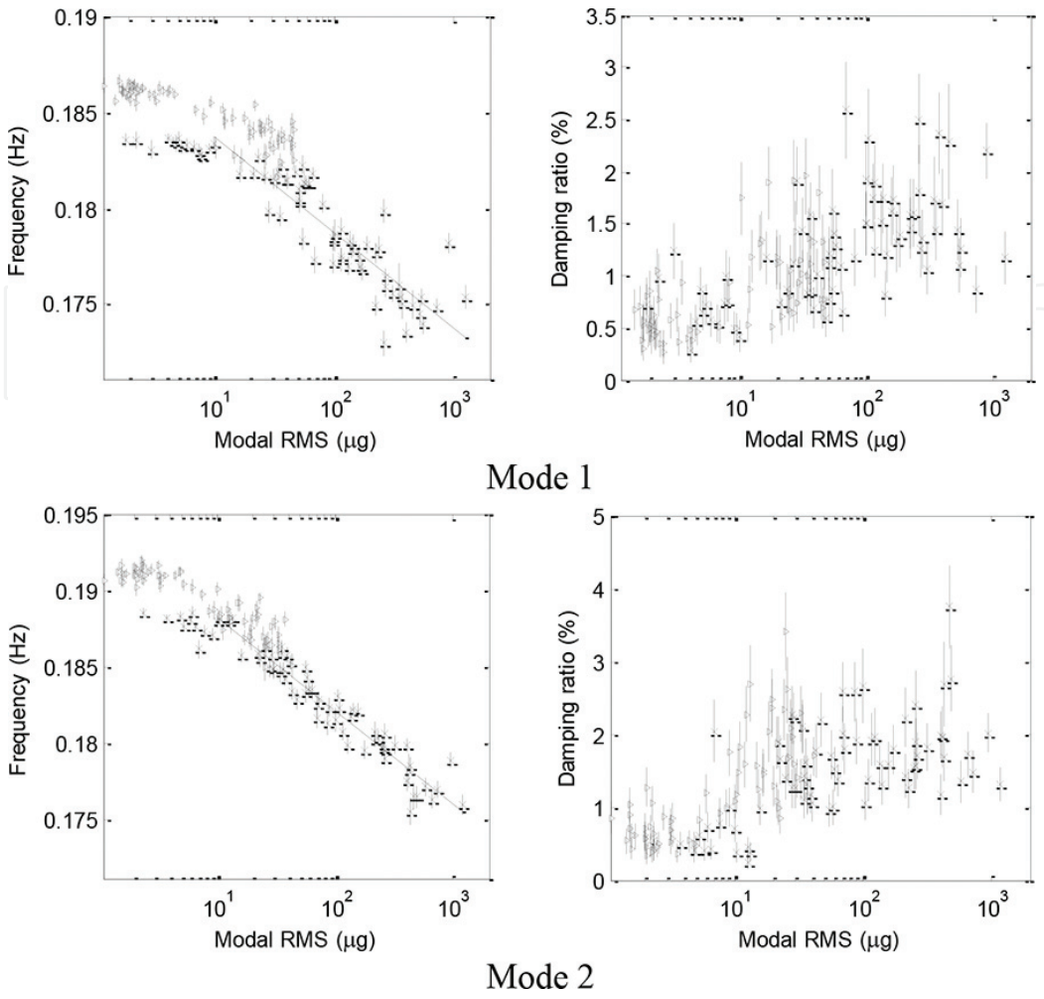

Figure 5. Identified modal frequency and damping ratio versus modal RMS of Building B (×: Koppu, ⊳: MS1).

triangle, respectively, denote the result for Typhoon Koppu and MS1. In the figures, each point is centred at the MPV with an error bar covering +/– one posterior standard derivation of the modal parameter. It is obvious from that the scatter in the MPV is significantly larger than those implied by the error bars, indicating some systematic dependence on the vibration amplitude.

There is an inverse trend between the natural frequency and the RMS value of the modal response, regardless of mode and building. Due to a season effect, the identified natural frequencies in Koppu (×) (in summer) are not the same with those in MS1 (⊳) (in winter) at low modal RMS. The natural frequency tends to decrease with the increase of modal RMS. One possible reason is the loosening of friction joints at sufficiently high vibration levels, which results in the reduction of stiffness. The right column of **Figures 4** and **5** shows a positive correlation between the damping ratio and RMS. Compared to that in the frequencies, the scatter is much bigger. The scatter in these figures can be due to limited identification precision, modelling error in the damping mechanism, modelling error in stationarity, unknown amplitude-dependence mechanism, etc. For the more detailed information of the study about the two super tall buildings, please refer to [6].

4. Canton Tower

The Canton Tower as shown in **Figure 6** situated in Guangzhou, China, is a super tall structure with a height of 610 m. It is composed of two tube-like structures, i.e., a reinforced concrete inner structure and a steel outer structure with concrete-filled-tube (CFT) columns.

The SHM system deployed on the Canton Tower is composed by more than 700 sensors, including anemometers, accelerometers, fibre optic strain and temperature sensors, global position system, and so on [24, 25]. Among them, 20 uni-axial accelerometers are installed on eight different cross-sections of the inner structure. On cross-sections 4 and 8, four accelerometers are instrumented at two locations for bi-axial measurement; while on each of the other cross-sections, two sensors are installed at two locations for uni-axial measurement. Sensors 01, 03, 05, 07, 08, 11, 13, 15, 17, 18 are deployed to collect the structural response in the short-axis direction, while sensors 02, 04, 06, 09, 10, 12, 14, 16, 19, 20 measure the structural response in the long-axis direction. The frequency range of accelerometers is DC to 50 Hz and amplitude range is ± 2 g. The 24-hour acceleration data were collected from 18:00, 20th January 2010 to 18:00, 21st January 2010 under normal wind condition. The sampling frequencies of acceleration are set to be 50 Hz.

As the last example, the 24-hour data were separated into 48 time windows with 30 minutes for each window. **Figure 7** shows the root PSD spectra of the structural responses of a typical

Figure 6. Overview of Canton Tower.

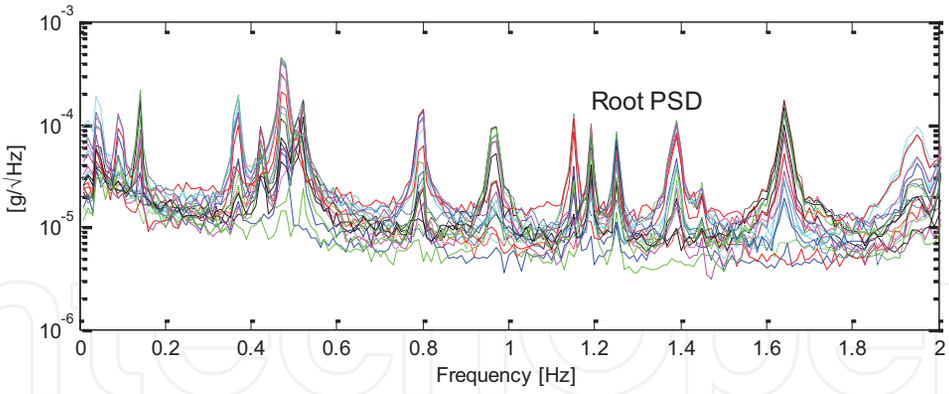

Figure 7. Power spectral density for a typical 30-minute window.

time window. Fifteen peaks can be observed below 2.0 Hz. The first mode is less than 0.1 Hz, and it is the foundational mode of the Canton Tower. In the operational modal analysis by the Fast Bayesian FFT method, all the 15 modes are identified. **Table 2** shows the identified modal parameters of the 15 modes. From the second to the ninth column, every two columns are considered as one group with first denoting the MPV and second denoting the associated posterior c.o.v. The c.o.v. of modal frequencies are quite small (less than 0.5%), implying that the MPVs are quite accurate. The damping ratios for this structure are small and only those of the first and fourth modes are higher than 1%. This is consistent with the results obtained in Ref. [24]. The posterior uncertainty of damping ratios is relatively high in comparison with that

Mode	Characteristics	f (Hz)	COV (%)	ζ (%)	COV (%)	S (μg^2/Hz)	COV (%)	Se (μg^2/Hz)	COV (%)
1	Bending	0.094	0.37	1.20	32.5	1.64	17.5	5.56	3.21
2	Bending	0.138	0.18	0.48	39.9	0.92	17.3	3.49	3.50
3	Bending	0.366	0.08	0.26	32.5	0.30	10.9	1.49	2.28
4	Bending	0.424	0.07	0.21	35.7	0.05	17.1	2.25	3.28
5	Bending	0.475	0.05	0.12	41.6	0.88	11.8	1.77	2.58
6	Torsion	0.506	0.04	0.10	46.4	0.05	21.5	8.83	4.00
7	Bending	0.522	0.07	0.27	29.1	0.19	15.6	2.52	3.01
8	Bending	0.796	0.05	0.23	23.2	0.08	7.8	0.81	1.61
9	Bending	0.966	0.06	0.36	17.5	0.06	7.6	0.65	1.50
10	Combined	1.151	0.03	0.13	26.8	0.01	11.7	0.63	2.35
11	Bending	1.191	0.03	0.11	29.1	0.01	12.9	0.84	2.53
12	Torsion	1.250	0.03	0.11	27.6	0.01	9.8	0.66	1.94
13	Bending	1.388	0.05	0.33	16.0	0.05	8.4	0.50	1.63
14	Bending	1.643	0.04	0.22	16.7	0.07	6.4	0.51	1.33
15	Combined	1.946	0.08	0.74	11.6	0.09	10.3	0.62	1.53

f: modal frequency; ζ: damping ratio; S: PSD of modal force; Se: PSD of prediction error.

Table 2. Identified modal parameters and the associated posterior uncertainty.

of modal frequencies, with an order of magnitude of a few tens' percent. The PSD of modal force and PSD of prediction error are all related to the excitation environment. The c.o.v. of the former is apparently larger than the c.o.v. of the latter.

Figures 8 and **9** show the identified mode shapes of the fifteen modes projected in short- and long-axis directions, respectively. As aforementioned, on cross-sections 4 and 8, four accelerometers were deployed for bi-axial measurement at two plane locations. With this information, the torsional behaviour of these modes can be investigated. From the mode shapes identified (omitted here), although the mode shapes of some modes in **Figures 8** and **9** are similar when projected in short- or long-axis direction, they are different in top view, i.e. Modes 6, 10, 12, 15 exhibit a significant torsional behaviour.

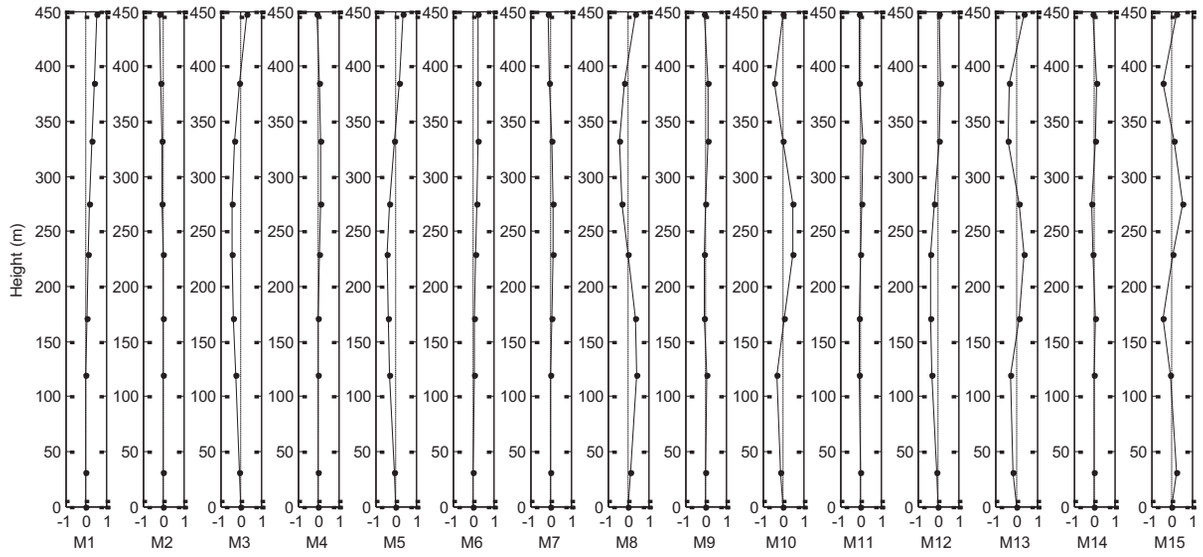

Figure 8. Identified mode shapes for the first 15 modes projected in short-axis direction.

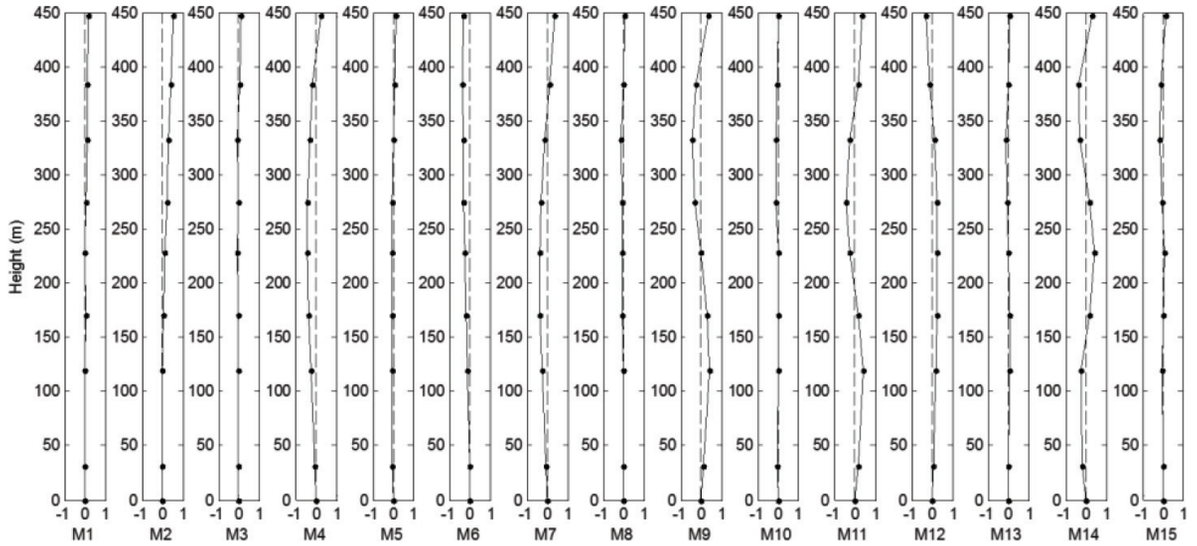

Figure 9. Identified mode shapes for the first 15 modes projected in long-axis direction.

To verify the results identified by the Fast Bayesian FFT method, the enhanced FDD method is used to identify the modal parameters using the same data. **Table 3** shows the identified modal frequencies and damping ratios. The identified modal frequencies for different modes are consistent with their counterparts identified by the Fast Bayesian FFT method. However, there is a larger discrepancy for the damping ratios. A noticeable difference can be observed between the two groups of results, implying that high uncertainty exists in the identified damping ratios, as shown by the large posterior c.o.v. of damping ratios obtained by the Fast Bayesian FFT method. For the more detailed information of the study about Canton Tower, please refer to [4].

Mode	Modal frequency (Hz)	Damping ratio (%)
1	0.094	2.48
2	0.138	1.33
3	0.366	0.46
4	0.424	0.32
5	0.475	0.29
6	0.506	0.28
7	0.522	0.43
8	0.796	0.46
9	0.965	0.64
10	1.151	0.16
11	1.191	0.16
12	1.250	0.16
13	1.390	0.34
14	1.642	0.27
15	1.948	0.86

Table 3. Modal parameters identified by enhanced FDD method.

5. Shanghai Tower

The Shanghai Tower (**Figure 10**) is a 124-story 632 m high super tall structure, situated in Lujiazui, Shanghai, China. The structure has eight electromechanical floor zones with six two-storey outrigger trusses together with eight boxy space circular trusses set along these different zones. It has a mega frame-tube-outrigger lateral resistant system, where the mega frame is composed by the boxy space circular truss and the giant column. To monitor the structural condition of the super tall building, an SHM system was instrumented on this structure. Many kinds of sensors were installed including accelerometers, temperature sensors, GPS, etc. A series of field vibration tests were conducted to investigate its modal parameters.

Figure 10. Overview of the building.

5.1. Field vibration tests in different stages

From April 2012 to December 2014, to study the modal parameters during construction, 15 ambient vibration tests were carried out over a period of two and a half years. **Table 4** shows the time to carry out the field test corresponding to the number of floors constructed. Two different locations were measured in each test. They were at the top of a core tube and the top of composite slabs after completion of concrete pouring. A series of finite element models (FEMs) (built by ETABS) of the first eight construction stages were also developed to perform comparison. The measured structures and the FEM model are shown in **Figure 11**.

When the main structure was finished, one field test was conducted to measure different corners of the tube to investigate the dynamic characteristics of a typical floor. For the convenience of sensor alignment and cables arrangement, 101th floor was selected since only the shear walls were constructed on this floor. It was planned to measure nine locations bi-axially,

Setup	**1**	**2**	**3**	**4**	**5**	**6**	**7**	**8**	**9**	**10**	**11**	**12**	**13**	**14**	**15**
Year/Month	12/04	12/07	12/08	12/10	13/01	13/03	13/05	13/07	13/08	13/12	14/02	14/03	14/07	14/10	14/12
Floors	55	68	71	81	94	102	111	120	125	125	125	125	125	125	125

Table 4. Measurement information.

Figure 11. Overview of buildings in different stages and finite element models, field test on a typical floor.

which are shown in **Figure 12**. It includes one location at the centre and the locations in the eight corners. With the help of core walls, sensor alignment was finished in half an hour.

In this test, only four uniaxial sensors were available, and so to finish the whole measurement, multiple setups were designed. Two reference channels were put in Location 1 to provide common information for mode shapes assembling and they were kept unchanged during the whole measurement. Based on the number of sensors and locations, eight different setups were

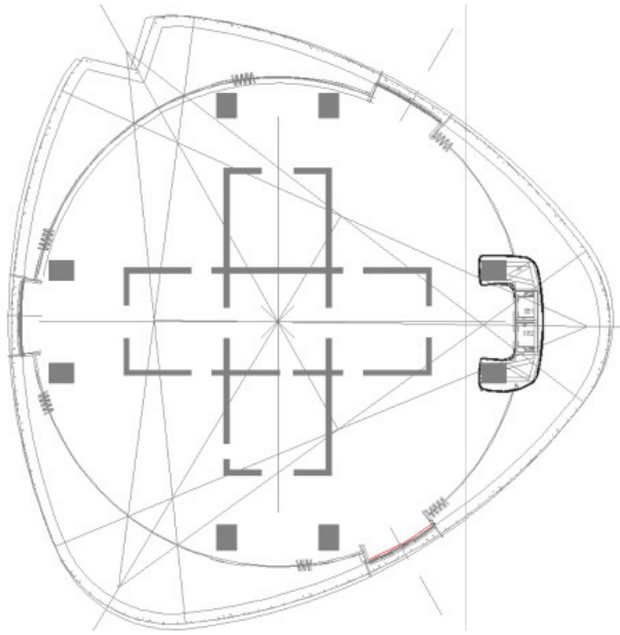

Figure 12. Setup plan.

arranged. The plans for these setups can be found in Ref. [26]. Forty minutes are required at least for each setup. Thirty minutes were used for data collection and the remaining 10 minutes were used for roving the sensor. It covered 10 am to 7 pm during a working day to finish the whole measurement with the sampling frequency of 2048 Hz. For the convenience of analysis, the measured data were decimated to a sampling frequency of 64 Hz.

5.2. Data analysis

Using the data collected in different construction stages, the variations of modal parameters were investigated. In each test, 20 minutes data in the Location 2 were analysed. **Figure 13** provides the identified results of natural frequencies and damping ratios for Modes 1 and 2. The MPV is denoted by a dot, while ±2 posterior standard deviations were expressed by an error bar. The MPV of natural frequencies decreases with the number of floors and the increasing speed tends to be stable after the main structure was finished. The posterior uncertainty of the natural frequency is small, and so the decrease of the natural frequency with the number of floors constructed is due to the structural height instead of identification error since the error bars among neighbouring setups have no overlap. For the damping ratios, the MPVs are all around or less than 1% and no obvious trend can be observed with the structural height. The posterior uncertainty of damping ratios is relatively large, which can be seen in **Figure 13**.

The identified results of the first two modes and the corresponding ones obtained from the FEM are shown in **Figure 14**. From the figure, it is seen that the two group results were consistent with each other, which implies that the influence of the increase of structural height

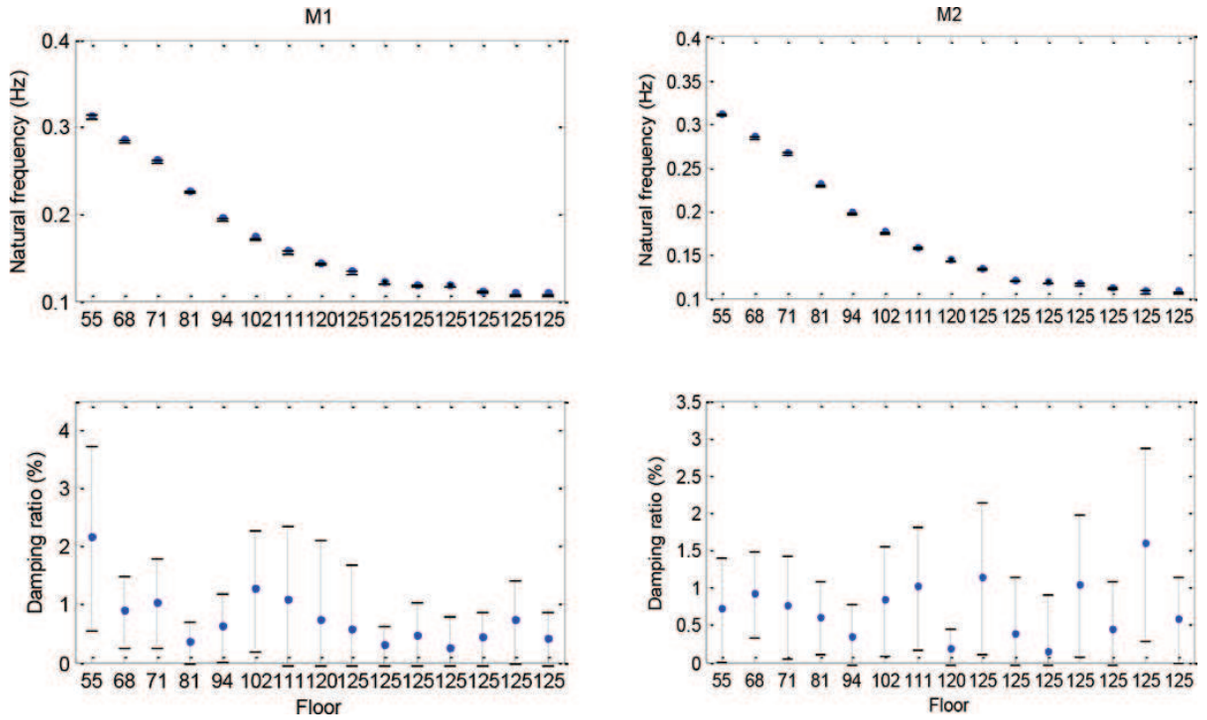

Figure 13. Modal parameters in different construction stages.

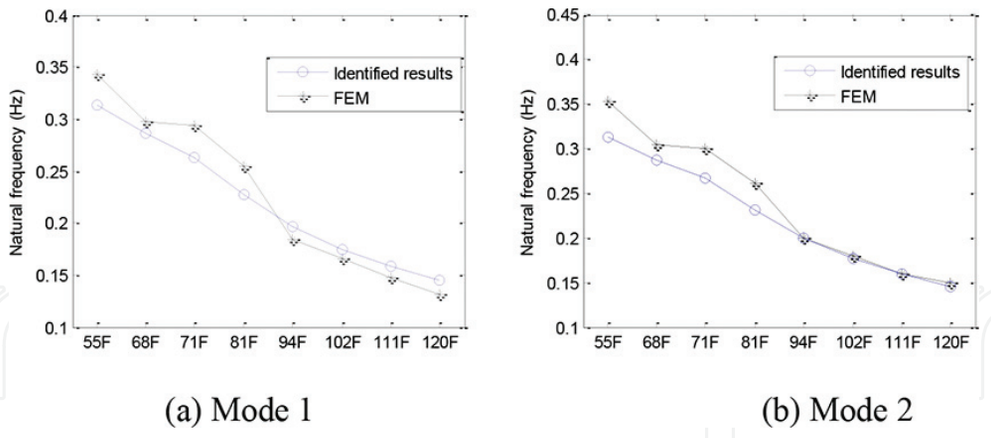

Figure 14. Comparison between the identified results and FEM results. (a) Mode 1 and (b) Mode 2.

on the reduction of natural frequency is reasonable. No obvious problem from the point of view of this modal parameter can be observed during construction.

Next, the data of the field test in a typical floor will be investigated. **Figure 15** plots the PSD spectra of the data in Setup 1. Eight obvious peaks can be observed from 0 to 1 Hz. The numbers near to each peak indicate the potential modes. There are two closely spaced modes (Modes 1 and 2) whose mode shapes can be predicted by the FEM model to be two transitional modes in x- and y-directions of the building, respectively. Therefore, to use the proposed multiple setups algorithm, the data in x- and y-directions were analysed separately to obtain the mode shapes. For Mode 3 to Mode 8, they can be taken as well separated, and so they are identified directly using the collected data.

The mode shapes of the first three identified modes were shown in **Figure 16**. Modes 1 and 2 are, respectively, two translational modes along the x- and y-directions. The third mode is a torsional mode and its torsion centre is at the centre of the tube. The mode shapes of Modes 4–6 are similar to Modes 1–3. Modes 7 and 8 (omitted here) are also, respectively, the two translational modes in the x- and y-directions. From the mode shapes, it is observed that although this super building was designed in a novelty manner, the mode shapes of the first eight modes are still all regular,

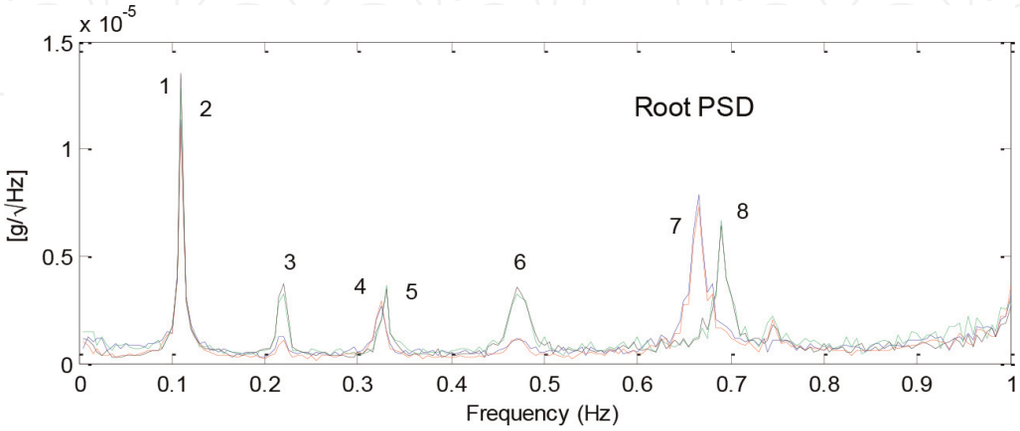

Figure 15. PSD spectrum of the data in Setup 1: (a) PSD spectra and (b) SVD spectra.

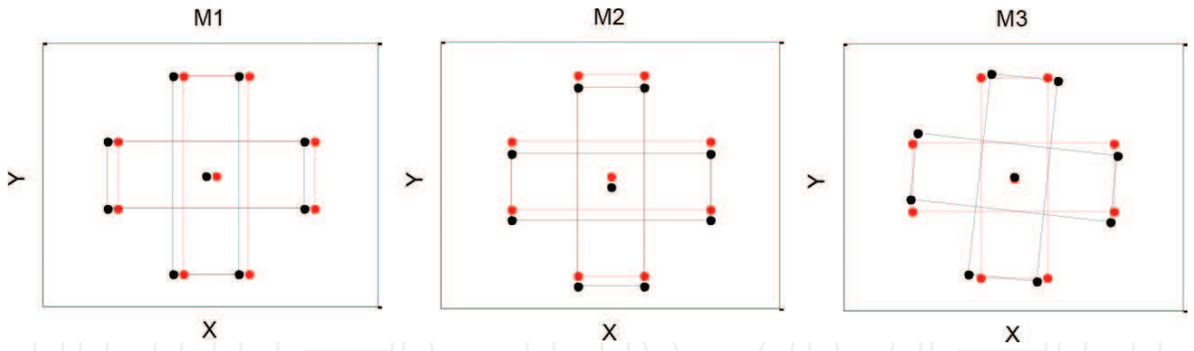

Figure 16. Identified mode shapes: Mode 1, Mode 2, and Mode 3.

i.e. two translational modes and then one torsional mode. **Table 5** gives the averaged posterior c.o.v. and the sample c.o.v. (=sample standard derivation/sample mean) of identified modal parameters for the first eight modes among different setups. The posterior c.o.v. tends to be larger than the sample c.o.v., while their orders of magnitude are still similar. These two quantities are well consistent with each other, although they can, respectively, reflect Bayesian and frequentist perspectives. For the more detailed information of the study about Shanghai Tower, please refer to [26].

Mode		1	2	3	4	5	6	7	8
f(%)	Pc.o.v.	0.37	0.34	0.23	0.18	0.35	0.14	0.18	0.21
	Sc.o.v.	0.48	0.37	0.27	0.17	0.40	0.21	0.12	0.67
z(%)	Pc.o.v.	57	46	38	48	48	25	26	32
	Sc.o.v.	88	48	53	41	62	31	27	33

Table 5. Posterior c.o.v. and sample c.o.v..

6. Conclusion

This chapter presents the work on the operational modal analysis of four super tall buildings including two super tall buildings situated in Hong Kong, Canton Tower and Shanghai Tower. A fast Bayesian method is used to perform the OMA. It is found that the Bayesian method can be well applied into these four field structures. The natural frequencies of the first fundamental mode of these four buildings are around 0.1 Hz, while the damping ratios are all around 1%. In addition to the most probable values of modal parameters, the associated posterior uncertainties are also investigated. The posterior c.o.v. of natural frequencies are usually small, indicating the identification of this quantity is accurate, while that of damping ratios are obviously larger than the natural frequencies. This is consistent with the common finding. The investigation in this chapter provides a reference for future OMA of super tall buildings, and the Fast Bayesian FFT method is a robust method having the potential to be used in other field structures.

Acknowledgements

The work in this paper was partly supported by grants from National Natural Science Foundation of China through Grant 51508413 and 51508407, Shanghai Pujiang Program (Grant No.: 15PJ1408600) and Fundamental Research Funds for the Central Universities (Grant No.:20161143).

Author details

Feng-Liang Zhang and Yan-Chun Ni*

*Address all correspondence to: yanchunni@gmail.com

College of Civil Engineering, Tongji University, Shanghai, China

References

[1] Chang PC, Flatau A, Liu SC. Health monitoring of civil infrastructure. Structural Health Monitoring. 2003;**2**(3):257–267

[2] Van der Auweraer H, Peeters B. International research projects on structural health monitoring: An overview. Structural Health Monitoring. 2003;**2**(4):341–358

[3] Ni YQ, Xia Y, Liao WX, Ko JM. Technology innovation in developing the structural health monitoring system for Guangzhou New TV Tower. Structural Control and Health Monitoring. 2009;**16**:73–98

[4] Zhang FL, Ni YQ, Ni YC, Wang YW. Operational modal analysis of Canton Tower by a fast frequency domain Bayesian method. Smart Structures and Systems. 2016;**17**(2):209-230

[5] Kijewski-Correa T, Kwon DK, Kareem A, Bentz A, Guo Y, Bobby A, Abdelrazaq A. Smartsync: An integrated real-time structural health monitoring and structural identification system for tall buildings. Journal of Structural Engineering, ASCE. 2013;**139**(10):1675–1687

[6] Au SK, Zhang FL, To P. Field observations on modal properties of two tall buildings under strong wind. Journal of Wind Engineering and Industrial Aerodynamics. 2012;**101**:12–23

[7] Li QS, Yi J. Monitoring of dynamic behaviour of super-tall buildings during typhoons. Structure and Infrastructure Engineering: Maintenance, Management, Life-Cycle Design and Performance. 2016;**12**(3):289–311

[8] Lam HF, Hu J, Yang JH. Bayesian operational modal analysis and Markov chain Monte Carlo-based model updating of a factory building. Engineering Structures. 2017;**132**:314–336

[9] Au SK, Zhang FL. Fundamental two-stage formulation for Bayesian system identification, Part I: General theory. Mechanical Systems and Signal Processing. 2016;**66**:31–42

[10] Zhang FL, Au SK. Fundamental two-stage formulation for Bayesian system identification, Part II: Application to ambient vibration data. Mechanical Systems and Signal Processing. 2016;**66**:43–61

[11] Au SK, Zhang FL, Ni YC. Bayesian operational modal analysis: Theory, computation, practice. Computers and Structures. 2013;**126**:3–14

[12] Peeters B, De RG. Stochastic system identification for operational modal analysis: A review. Journal of Dynamic Systems Measurement and Control-Transactions of the ASME. 2001;**123**(4):659–667

[13] Brincker R, Zhang L, Anderson P. Modal identification of output-only systems using frequency domain decomposition. Smart Materials and Structures. 2001;**10**:441–455

[14] Yuen KV. Bayesian Methods for Structural Dynamics and Civil Engineering. New York: Wiley; 2010

[15] Yan WJ, Katafygiotis LS. A two-stage fast Bayesian spectral density approach for ambient modal analysis. Part I: most probable values and posterior uncertainty. Mechanical Systems and Signal Processing. 2015;**54**:139–155

[16] Au SK. Fast Bayesian FFT method for ambient modal identification with separated modes. Journal of Engineering Mechanics, ASCE. 2011;**137**:214–226

[17] Au SK. Fast Bayesian ambient modal identification in the frequency domain, Part I: Posterior most probable value. Mechanical Systems and Signal Processing. 2012;**26**:60–75

[18] Au SK. Fast Bayesian ambient modal identification in the frequency domain, Part II: posterior uncertainty. Mechanical Systems and Signal Processing. 2012;**26**:76–90

[19] Au SK, Zhang FL. Fast Bayesian ambient modal identification incorporating multiple setups. Journal of Engineering Mechanics, ASCE. 2012;**138**(7):800–815

[20] Zhang FL, Au SK, Lam HF. Assessing uncertainty in operational modal analysis incorporating multiple setups using a Bayesian approach. Structural Control and Health Monitoring. 2015;**22**(3):395–416

[21] Au SK, Ni YC. Fast Bayesian modal identification of structures using known single-input forced vibration data. Structural Control and Health Monitoring. 2014;**21**(3):381–402

[22] Zhang FL, Ni YC, Au SK, Lam HF. Fast Bayesian approach for modal identification using free vibration data, Part I - Most probable value. Mechanical Systems and Signal Processing. 2016;**70-71**:209–220

[23] Ni YC, Zhang FL, Lam HF, Au SK. Fast Bayesian approach for modal identification using free vibration data, Part II - Posterior uncertainty and application. Mechanical Systems and Signal Processing. 2016;**70-71**:221–244

[24] Chen WH, Lu ZR, Lin W, Chen SH, Ni YQ, Xia Y, Liao WY. Theoretical and experimental modal analysis of the Guangzhou New TV Tower. Engineering Structures. 2011;**33**:3628–3646

[25] Ni YQ, Xia Y, Lin W, Chen WH, Ko JM. SHM benchmark for high-rise structures: A reduced-order finite element model and field measurement data. Smart Structures and Systems. 2012;**10**(4):411–426

[26] Zhang FL, Xiong HB, Shi WX, et al. Structural health monitoring of Shanghai Tower during different stages using a Bayesian approach. Structural Control and Health Monitoring. 2016;**23**(11):1366–1384

IntechOpen